Socially Aware Navigation for a Walking-Assist Robot in a Pedestrian-Rich Environment

CHIEN-YU SU[1], SHIH-HSING LIU[1], CHUN-HSU KO[2] AND KUU-YOUNG YOUNG[1,+]
[1]*Department of Electrical Engineering*
National Yang Ming Chiao Tung University
Hsinchu, 300 Taiwan
[2]*Department of Electrical Engineering*
I-Shou University
Kaohsiung, 840 Taiwan.
**Correspondence: kyoung@nycu.edu.tw; Tel.: +886-3-5712121-54366*

As society continues to age, more elderly people experience mobility difficulties. With the walking-assist robot deemed to be helpful for their motion guidance and physical support, in this paper, we further extend its application from a home or nursing house, which may be less challenging, to more crowded environments in our daily lives. Consequently, it demands a path planner that can efficiently deal with moving pedestrians, and also be socially aware. By taking into account the comfort of both the user and pedestrians, the concept of personal space is introduced, which is in accordance with the social norms, such as walking on the left or right, not crossing in front of others, and following instead of passing a group. Furthermore, because the passive type of walking-assist robot was adopted for safety concerns, which relies mainly on the user's applied force to move, the corresponding passive control strategy is developed to realize the proposed navigation scheme. Extensive simulations and then a field study on our campus cafeteria are conducted for demonstration.

Keywords: socially aware navigation, walking-assist robot, personal space, passive control

1. INTRODUCTION

Owing to an aging society, a growing number of people suffer from mobility problems, thus soliciting the development of various kinds of walking aids [1]. Among them, the walking-assist robot is favored for being able to entice exercise, when the elders can still walk, in addition to its support for balance and motion guidance [2]. However, its current application is limited to a less challenging home or nursing house environment, as it is not that effective when interacting with a larger number of incoming persons. Motivated by it, in this paper, we propose equipping the walking-assist robot with a novel navigation scheme, so that it can be applied to a general public space, which may in turn encourage the elderly for more social engagement.

The proposed navigation scheme mainly consists of a path planner that is able to derive a feasible path among the moving pedestrians in a socially aware manner, and a control strategy capable of governing the robot to follow that path. Including social norms in path planning should benefit robot-human interaction, which is especially desirable for the assistive types of robots. Kylberg et al. pointed out that even if robots possess a highly ef-

fective collision avoidance ability, the absence of socially reassuring cues in their interactions could impact human comfort [3]. Rios-Martinez also mentioned that adherence to social customs can let the coexistence of humans and robots be more natural [4]. Meanwhile, the demand for social compliance will certainly complicate this already highly challenging task of searching for a collision-free path in a crowded space.

Previous research on socially compliant navigation has primarily focused on mobile robots, with limited applications to walking-assist robots. Nevertheless, these studies have provided valuable insights into how walking-assist robots can handle social interaction. Chen et al. proposed applying deep reinforcement learning to derive collision-free paths by analyzing the future states of nearby pedestrians; however, their method requires high computational costs, posing certain limitations for applications demanding real-time performance [5]. Everett et al. employed deep learning frameworks to train collision avoidance algorithms in multi-pedestrian environments without assuming specific behavioral rules, while this approach may generate unnatural navigation trajectories when encountering new scenarios [6]. Mehta et al. proposed a navigation scheme based on multi-policy decision-making for dynamic, unstructured environments, but it demands substantial computational resources [7]. Ferrer and Sanfeliu developed a human behavior estimator based on the social force model for environments with dynamic crowds and moving obstacles, while limitations persist when handling highly crowded scenarios [8]. Boldrer et al. combined the potential field method with limit cycles to guide robots in avoiding pedestrians' personal space, but this approach is susceptible to local minima, affecting navigation stability [9].

Among these researches, although learning approaches excel in adapting to social norms, their high computational costs and scene dependency limit their feasibility in real-time applications. In contrast, model-driven approaches offer higher computational efficiency, making them more suitable for walking-assist robots operating in crowded environments. In this study, we opt for a model-based approach, combining it with flexible personal space modeling, starting from basic types of social norms to achieve an efficient navigation solution. Extending from our previous work [10], which had included spatial and visual comfort in path planning in a static environment for an active type of walking-assistive robot, the proposed scheme will move on to deal with dynamic obstacles, and can be applied to that of a passive type for safety concerns [11].

Relative to that of autonomous robotic vehicles, the walking-assist robot poses a different kind of challenge in its close bondage with the user, while that of the passive type further raises its own in moving the robot only via the applied force from the user, which would then trigger the brakes for steering, instead of through active guidance [12]. In previous related research, Andreetto et al. introduced an authority-sharing approach, in which the motors were deactivated as the robot followed a planned path, and activated when it deviated [13]. Later, they further enhanced the system by incorporating vibrating wristbands to notify users of deviations [14]. In responding to the challenge, we come up with a new passive control strategy to realize the path derived from the proposed socially aware path planner. The effectiveness of the proposed navigation scheme is demonstrated via a series of simulations that involve various crowd scenarios and also experiments at our

campus cafeteria during rush hour. Comparing with previous approaches, we consider the proposed scheme to have the following merits:

- A novel path planner that is able to find a socially-aware collision-free path in a crowded environment is developed. To the best of our knowledge, this is the first attempt to include social norms into path planning in a pedestrian-rich environment for the walking-assist type of robot.
- A new passive control strategy that responds well to the situations resulting from the social norms, such as sharp turns or sudden stops, is developed, so that it can govern the walking-assist robot to follow the planned path effectively and smoothly.
- The proposed scheme is well integrated to be capable of conducting a field study at our campus cafeteria, with its performance compared to the state-of-the-art approaches via simulations.

The rest of this paper is organized as follows: Sec. 2 describes the proposed navigation system, including the description of the employed walking-assist robot, and the modules of pedestrian tracking, personal space generation, trajectory planning, and passive control. Simulations and experiments conducted in the campus cafeteria are reported in Sec. 3. Finally, concluding remarks are given in Sec. 4.

2. PROPOSED NAVIGATION SYSTEM

Fig. 1 shows a conceptual diagram of the proposed navigation scheme, including the modules for pedestrian tracking, personal space generation, trajectory planning, and passive control. The walking-assist robot employed in this study is named as i-Go, which is an advanced version of that previously developed in our laboratory [12], described in Section 2.1. In Fig. 1, as the user maneuvers the walking-assistive robot to enter a crowded environment for daily activities, sensors, such as a camera and Lidar, will be activated to collect information of the incoming pedestrians and others, which will then be forwarded to the pedestrian tracker for analysis, described in Section 2.2. With the environmental status available, the personal space generator will then determine the personal space adhering to social norms that corresponds to each individual, described in Section 2.3, and also build a cost map for the path planner to derive a socially compliant path, described in Section 2.4. In turn, the passive controller will be employed to ensure successful execution of the planned path via salient management of the demands from both the user and social norms, described in Section 2.5.

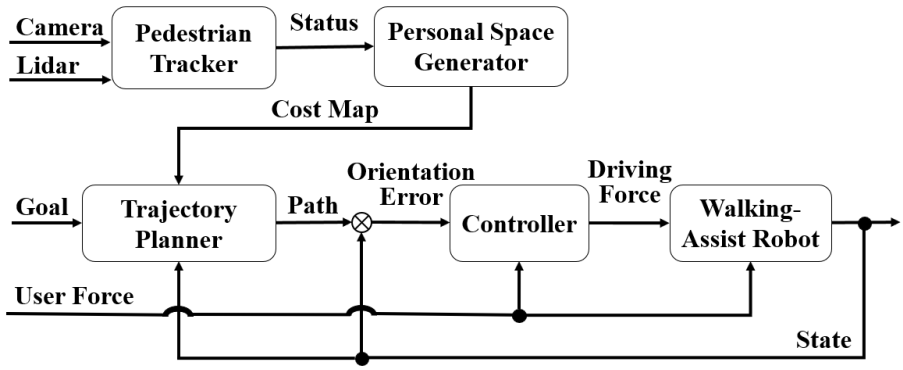

Fig. 1. A conceptual diagram for the proposed navigation scheme.

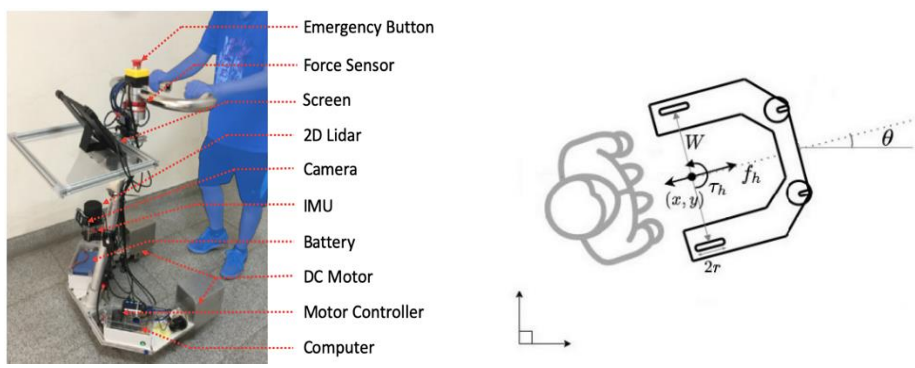

(a) Outlook (b) Chassis

Fig. 2. The walking-assist robot i-Go and its chassis: (a) outlook and (b) chassis.

2.1 Walking-Assist Robot

Fig. 2(a) shows the outlook of the walking-assist robot, named as i-Go, which is at a height of 1.1 m, with left and right auxiliary wheels attached with corresponding DC motors. Several sensors are equipped, including a six-axis force sensor (WACOH) for user's applied force measurement, 2D camera (Logitech) for pedestrian detection, 2D Lidar (YDLIDAR) for obstacle detection and robot positioning, and IMU (Sparkfun) also for robot positioning. The Jetson Xavier NX embedded computer (NVIDIA) was adopted as the computing platform, and an emergency stop switch was installed for safety considerations. During task execution, the user first applies force to maneuver the i-Go, which is measured by the force sensor. The measured force, along with the visual information of the pedestrians and obstacles, are then forwarded to the proposed scheme to derive a socially compliant path for navigation, which is further processed by the passive controller to generate proper braking torques for motion assistance.

Fig. 2(b) shows the chassis of i-Go with a rotational center (x, y) and a heading angle θ in Cartesian coordinates. Assuming the walking-assist robot moves on a flat surface without wheel slip, we can obtain [11]

$$\dot{q} = \begin{bmatrix} cos\theta & 0 \\ sin\theta & 0 \\ 0 & 1 \end{bmatrix} V \tag{1}$$

where $q = [x, y, \theta]^T$, V is the vector of the speed v and angular speed ω, i.e., $V = [v, \omega]^T$. By further assuming the walking-assist robot is symmetric, its dynamic equation can be derived as

$$\dot{V} + \begin{bmatrix} \frac{D_{xy}}{m} & 0 \\ 0 & \frac{D_\theta}{J} \end{bmatrix} V = \mathbf{A}\tau_m + \begin{bmatrix} \frac{1}{m} & 0 \\ 0 & \frac{1}{J} \end{bmatrix} F_h \tag{2}$$

with

$$\mathbf{A} = \begin{bmatrix} \frac{1}{mr} & \frac{1}{mr} \\ \frac{W}{2Jr} & -\frac{W}{2Jr} \end{bmatrix},\ \tau_m = \begin{bmatrix} \tau_r \\ \tau_l \end{bmatrix},\ F_h = \begin{bmatrix} f_h \\ \tau_h \end{bmatrix} \tag{3}$$

where f_h and τ_h stand for user's applied force and torque, respectively, τ_r and τ_l for the torque generated by right and left wheels, respectively, $D_{xy} = 45.0\ (\mathrm{N \cdot s/m})$ and $D_\theta = 20.0\ (\mathrm{N \cdot m \cdot s/rad})$ as the damping parameters, $r = 0.0625\ \mathrm{m}$, $W = 0.6\ \mathrm{m}$, $m = 30\ \mathrm{kg}$, and $J = 10.0\ (\mathrm{kg \cdot m^2})$ as the wheel radius, distance between the rear wheels, mass of the robot, and its moment of inertia, respectively. This dynamic equation will then be utilized to derive the passive control strategy in Sec. 2.5.

2.2 Pedestrian Tracking

The pedestrian tracker is used to acquire the status of the pedestrians via close monitoring of their movements in a crowded environment, intended for the following personal space generation and path planning. It thus needs to be able to differentiate the pedestrians from the static obstacles, and also determine their directions relative to the robot. Fig. 3 shows its process. The images of the pedestrians obtained by the 2D camera are first bounded by using the Yolov4_tiny neural network [15], which are assigned with directional vectors from the robot to the *m* pedestrians, denoted as $\vec{U}_\mathrm{d} = [\vec{u}_\mathrm{d}^1, \vec{u}_\mathrm{d}^2, \cdots, \vec{u}_\mathrm{d}^m]$. Meanwhile, the point clouds obtained from the 2D Lidar are clustered into groups by using the DBSCAN (density-based spatial clustering of applications with noise algorithm) [16], which are assigned with vectors that identify the distances and directions of each Lidar cluster (including obstacles and pedestrians), denoted as $\vec{U}_\mathrm{s} = [\vec{u}_\mathrm{s}^1, \vec{u}_\mathrm{s}^2, \cdots, \vec{u}_\mathrm{s}^n]$. While both $\vec{U}_\mathrm{d}$ and $\vec{U}_\mathrm{s}$ are available, the Hungarian algorithm [17], commonly used for solving assignment problems, is then employed to accurately allocate the cluster to their respective pedestrian with the coordinates $\boldsymbol{C}$. As the pedestrians may be obstructed by objects or other pedestrians during the tracking process, the AB3DMOT (A Baseline for 3D Multi-Object Tracking) [18], known for its effectiveness in 3D multi-object tracking, is then used to estimate the pedestrians' positions, directions, and velocities. Finally, the state vectors of the pedestrians S_h in the global coordinate system, including their position, direction, and velocity, are derived from a series of $\boldsymbol{C}$:

$$S_h = \left[s_h^1, s_h^2, \ldots, s_h^i\right] \tag{4}$$

where $s_h^i = [x_0, y_0, \theta, v]$, denoting the state of the i^{th} pedestrian, with x_0 and y_0 representing the pedestrian's position, as θ and v stand for the direction and velocity, respectively.

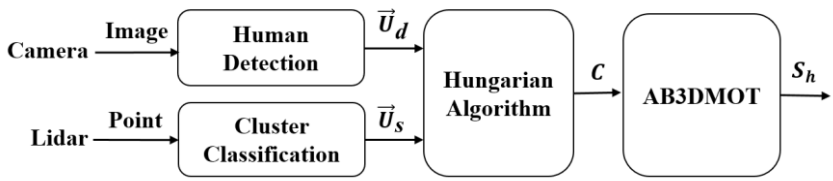

Fig. 3. The pedestrian tracking process.

2.3 Personal Space Generation

The inclusion of social awareness into path planning can be realized basically by surrounding a person with a zone as a buffer, referred to as a personal space [10]. It started with simply using a circle, as shown in Fig. 4(a) [19]. To respond to the situation that people may experience higher psychological stress when facing the incoming object, Batista et al. suggested using an asymmetric Gaussian function (AGF), so that more space should be allocated in front, as shown in Fig. 4(b) [20]. To meet the requirements for the specific social norms, in this paper, we further propose a new form of personal space, AGF-SN (asymmetric Gaussian function-social norm), that allows the Gaussian function to vary its sizes in various portions accordingly, as shown in Fig. 4(c).

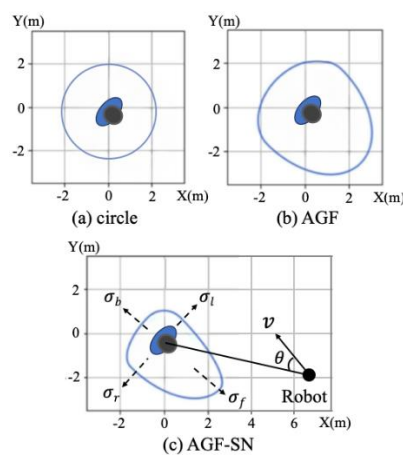

Fig. 4. Three kinds of social spaces: (a) circle, (b) AGF, and (c) AGF-SN.

(a) adhering to the walking left/right convention (b) yielding when crossing (c) following behind a group

Fig. 5. Three basic social norms (right-handed rule): (a) adhering to the walking left/right convention, (b) yielding when crossing, and (c) following behind a group.

Fig. 5 shows the three basic types of social norms selected for the robot to abide by, including adhering to the walking left/right convention, yielding when crossing, and following behind a group. In response, we propose the AGF-SN, which is designed to be able to vary its sizes in the front, back, and two sides, and also according to the approaching speeds of the pedestrians. The AGF-SN is formulated by using the asymmetric Gaussian function, but with much flexibility in its shape variation to comply with social norms. Referring to Fig. 4(c), for each point (x, y) within the personal space described by AGF-SN, the function $f_p(x, y)$ that derives its corresponding cost when facing an incoming pedestrian is formulated as

$$f_p(x, y) = e^{-(a(x-x_0)^2+2b(x-x_0)(y-y_0)+c(y-y_0)^2)} \tag{5}$$

where (x_0, y_0) is the position of the pedestrian, and a, b, and c are the functions of σ_f, σ_b, σ_r, σ_l, and θ for determining its shape, size, and orientation, with θ indicating the direction of the robot relative to the pedestrian, and σ_f, σ_b, σ_r, and σ_l the variance for its front, back, right, and left direction, respectively.

To respond the social norms of adhering to the left(right) walking convention, yielding when crossing, and following behind a group, the strategy is to choose smaller σ_r (σ_l) and σ_b, so that $f_p(x, y)$ will come up with lower costs in the left(right) and back sides of the space, prompting the robot to obey these rules. The values of these parameters may also be adjusted along with the increase(decrease) of the pedestrian's movement speed. During our experiments, we set $\sigma_b = 0.3\sigma_f$, $\sigma_r = 0.6\sigma_f$, $\sigma_l = 0.3\sigma_f$, and σ_f to be 1 by assuming the average pedestrian speed to be 0.5 m/s. These parameters were suitable for our experiments under the walking-right convention, while they can be adjusted to fit different social norms and working environments.

Meanwhile, for the case that the pedestrian stands still, we let $f_p(x, y)$ become symmetric by setting $a = c$ and $b = 0$, as users' moving directions are unknown. As for static obstacles, such as walls and tables, the symmetric Gaussian function is also used, but with smaller variances for their non-human nature. By integrating all space costs, it allows for

the creation of a cost map $\mathcal{M}$, with the cost for each of its grid cells adjusted to range from 0 to 1.

2.4 Trajectory Planning

Navigating a robot in a crowded environment is very challenging, particularly with the social norms to adhere to. The learning approach, such as deep reinforcement learning, has shown its potential in dealing with complex environments, but may result in unnatural trajectories when encountering previously unseen scenarios [5-6]. The potential field approach is capable of overcoming unknown scenes through its intuitiveness, while facing the possibility of getting stuck in local minima [7]. Meanwhile, the dynamic window approach is deemed to be effective for dynamic obstacle avoidance, which is at the expense of high computational load [21].

Due to real time consideration and limited computational resources on the walking-assist robot, our design concept is first to plan a shortest path $\mathcal{P}$ to reach the goal *G* under the social norm constraint based on the cost map $\mathcal{M}$ derived in Sec. 2.2 above. The robot should follow $\mathcal{P}$, except when the incoming pedestrian(s) blocks the path within its sensing distance (set to be around 5 m). It would detour to avoid them, and then return back to $\mathcal{P}$. Following the concept, we chose a relatively simple A* algorithm [22] to plan path $\mathcal{P}$, with the cost $\mathcal{F}$ that considered social norms, derived to be

$$\mathcal{F} = G + \mathcal{H} + k \cdot I \tag{6}$$

where G stands for the cost for movement from the starting point to a specified grid cell, $\mathcal{H}$ the estimated cost from that cell to the destination, I the cost for the cell in the cost map corresponding to social norms $\mathcal{M}$ derived in Section 2.2, and k the weight.

For the situation that a pedestrian is detected to get into the way, the planner will search for a temporary goal within the range of 0°~180° at a 10° interval, which is determined by considering both its cost on map $\mathcal{M}$ and distance to goal *G*. Because the walking-assist robot is not meant to move fast, the proposed planner serves well, as demonstrated by the simulations and experiments later.

2.5 Passive Control

To ensure that the walking-assist robot can smoothly follow the planned path derived above, especially under the circumstance that sharp turns or sudden stops may occur due to compliance with social norms, a new passive controller is proposed based on that previously developed in our laboratory [11]. Fig. 6 shows the scene in which the walking-assist robot is guiding a user to follow a desired path. The proposed controller is intended to minimize both the orientation error $\tilde{\theta} = \theta - \psi$, i.e., the angle between the robot and trajectory $\mathcal{P}$, and the position error d, i.e., the shortest distance from the robot to $\mathcal{P}$. With a slow-moving robot, the orientation error should be small, so that their derivatives can be derived as

$$\dot{\tilde{\theta}} = \tilde{\omega} = \omega - \omega_d, \; \dot{d} = v \cdot \tilde{\theta} \tag{7}$$

where $\tilde{\omega}$, ω, and ω_d are the rotational velocity error, actual and desired rotational velocities, respectively, and v is the linear velocity.

To respond to possible sharp turns due to social norm adherence, we propose adding an inhibitory force f_{inh} to slow down robot's speed in a smooth manner. For this purpose, the magnitude of f_{inh} is set to be zero when there is no orientation error ($\tilde{\theta}$), and gradually increases until $\tilde{\theta}$ reaches π/4. Accordingly, as shown in Fig. 7, f_{inh} is chosen to be

$$f_{inh} = -f_h/(1 + \exp(-40|\tilde{\theta}|/\pi + 5)) \tag{8}$$

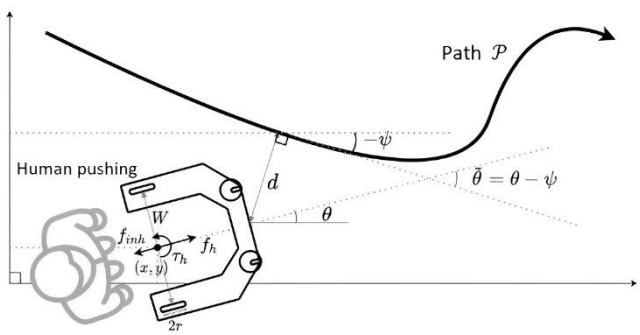

Fig. 6. The walking-assist robot is guiding a user to follow the desired path.

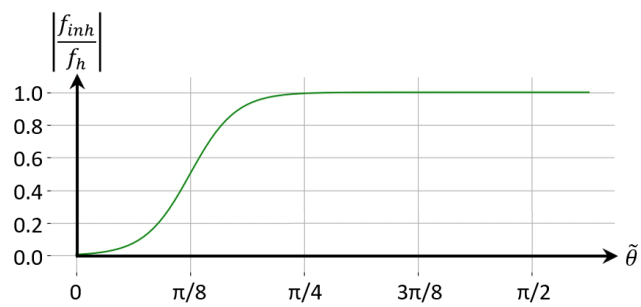

Fig. 7. Illustration for f_{inh} vs. $\tilde{\theta}$.

With f_{inh} included and considering the dynamic equation in Eq.(2), we set up the control law by choosing τ_m to be

$$\tau_m = \mathbf{A}^{-1}\begin{bmatrix} f_{inh}/m \\ \frac{D_\theta \omega}{J} - \frac{\tau_h}{J} - k_1\dot{\tilde{\theta}} - k_2\tilde{\theta} + \dot{\omega_d} \end{bmatrix} \tag{9}$$

where k_1 and k_2 represent control gains, with both greater than 0. By substituting (9) into (2), it leads to

$$\begin{bmatrix}\dot{v}\\ \dot{\omega}\end{bmatrix}+\begin{bmatrix}\frac{D_{xy}}{m} & 0\\ 0 & \frac{D_\theta}{J}\end{bmatrix}\begin{bmatrix}v\\ \omega\end{bmatrix}=\begin{bmatrix}\frac{f_{inh}}{m}\\ \frac{D_\theta\omega}{J}-\frac{\tau_h}{J}-k_1\dot{\tilde{\theta}}-k_2\tilde{\theta}+(\dot{\omega}-\dot{\hat{\omega}})\end{bmatrix}+\begin{bmatrix}\frac{1}{m} & 0\\ 0 & \frac{1}{J}\end{bmatrix}\begin{bmatrix}f_h\\ \tau_h\end{bmatrix} \quad (10)$$

After rearrangement, we can obtain

$$\ddot{\tilde{\theta}}+k_1\dot{\tilde{\theta}}+k_2\tilde{\theta}=0 \quad (11)$$

With k_1 and k_2 positive, orientation error $\tilde{\theta}$ should converges to zero. And, via Eq.(7), we can also obtain that $\dot{d}=v\cdot\tilde{\theta}$ converges to zero. Since the planned path starts at the robot's current position, with the initial position error being zero, the position error d should converge to a small value, demonstrating the stability of the proposed control law.

Here, we propose another controller, which is intended for robot autonomous navigation. The reason is that we intend to compare the performance of the proposed navigation scheme with those related state-of-the-art methods, while most of them have been applied to autonomous robotic vehicles. Our strategy is to let the walking-assist robot behave like an autonomous mobile one, i.e., it is without the governance from the user. Consequently, by removing user's applied force F_h, the dynamic equation in Eq.(5) becomes

$$\dot{V}+\begin{bmatrix}\frac{D_{xy}}{m} & 0\\ 0 & \frac{D_\theta}{J}\end{bmatrix}V=\mathbf{A}\tau_m \quad (12)$$

By selecting v_{pref} as the desired velocity for this mobile robot and applying the similar concept on designing f_{inh} in Eq.(8) for smoothing the impact from sharp turning, we come up with a corresponding control law by choosing τ_m to be

$$\tau_m=\mathbf{A}^{-1}\begin{bmatrix}\frac{D_{xy}v}{m}-k_1\left(v-v_{pref}\right)-\frac{v_{pref}}{1+\exp(-40|\tilde{\theta}|/\pi+5)}\\ \frac{D_\theta\omega}{J}-k_1\dot{\tilde{\theta}}-k_2\tilde{\theta}+\dot{\omega}_d\end{bmatrix} \quad (13)$$

where k_1 and k_2 are set to be the same as that for the walking assist robot. The stability of this controller can be proved following the similar procedure above.

3. SIMULATIONS AND EXPERIMENTS

We conducted a series of simulations and experiments based on using the i-Go to evaluate the performance of the proposed navigation scheme, including a comparison with the state-of-the-art methods and a field study at our campus cafeteria during rush hour. For simulations, we first used Solidworks to build a proportional model of the i-Go, shown in Fig. 8, including all components and sensors, and then Gazebo 9 for rendering the corresponding functions, such as sensing and control, in addition to the working environment.

For pedestrian emulation, the Pedsim_ROS library [23] was utilized to furnish each pedestrian with a human-like behavior [24]. We took into account the uncertainty of information processing, sensing noise, etc., and also considered the situations that might lead to misjudgment, such as the case that pedestrians were occluded by others, to make the simulated environment more realistic.

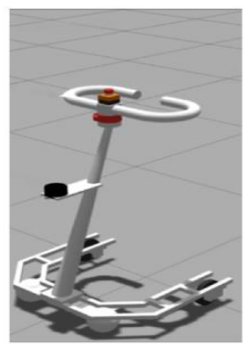

Fig. 8. The virtual walking-assistive robot used in the simulations.

3.1 Comparison with State-of-the-Art Methods

The first set of simulations were intended to compare the performance of the proposed navigation scheme with that of the state-of-the-art methods, including the Optimal Reciprocal Collision Avoidance (ORCA) approach based on the concept of velocity obstacle [25], and the two reinforcement learning approaches reviewed in the introduction, LM-SARL [5] and LSTM-RL [6], in addition to our previous approach on comfort-based motion guidance (CBMG) [10] and that using the asymmetric Gaussian function (AGF) to formulate personal space for social navigation [20]. Because most of the methods were developed for autonomous navigation, we let i-Go behave like an autonomous mobile robot during simulations, and adopted the control law in Eq. (13) for the proposed navigation scheme.

We developed the simulated environment to be similar to that used in [5][6], in which the pedestrians were randomly distributed on a circular path of 8 m in diameter, as shown in Fig. 9. They moved in a manner that might cross each other, and the robot needed to pass them to reach the goal on the other end. Both pedestrian and robot speeds were set to be 0.5 m per second to allow more interaction, with an angular velocity of 0.5 radian per second for the robot. A total of 200 trials were conducted and the number of pedestrians selected to be 4 and 8. The results are listed in Table 1, including the time for the robot to reach the destination, average minimum distance between pedestrians and the robot, and the number of navigation failure. Referring to Table 1, the CBMG led to a most comfortable path for the pedestrians with a largest average shortest distance between the pedestrian and robot, but it also spent the longest time to reach the destination for its conservative nature. The AGF exhibited the second-best time efficiency, that might be attributed to the introduction of the personal space. LSTM-RL had the highest failure rate, while ORCA and LM-SARL had mediocre performance. Meanwhile, the results show that the proposed scheme achieved a better balance between time efficiency and pedestrian comfort, as it

was with a more flexible personal space and a path planner was capable of locating a shorter path among the crowd.

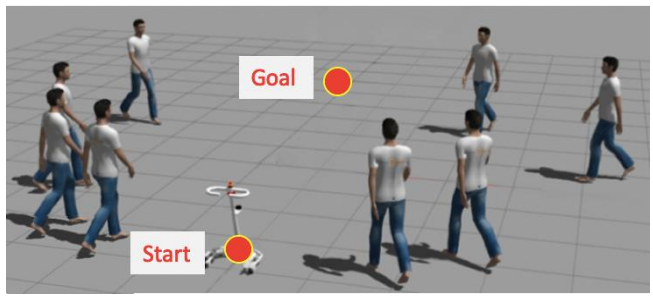

Fig. 9. Simulation scene for comparison with the state-of-the-art methods.

Table 1. Simulation results for autonomous navigation

Method	Average time (s)	Average shortest distance to pedestrian (m)	Failure (collision, timeout)
	4 pedestrians		
ORCA	20.2	1.10	2.5 (1.5, 1.0)
LM-SARL	20.2	0.99	3.5 (2.5, 1.0)
LSTM-RL	26.3	0.91	35.0 (10.5, 24.5)
CBMG	20.5	**1.20**	2.5 (0.0, 2.5)
AGF	19.7	1.07	**1.0 (1.0, 0.0)**
Proposed scheme	**19.3**	1.05	**1.0 (1.0, 0.0)**
	8 pedestrians		
ORCA	21.5	1.04	3.0 (0.5, 2.5)
LM-SARL	23.2	1.04	9.0(8.0, 1.0)
LSTM-RL	27.2	0.85	45.0 (36.5, 8.5)
CBMG	23.3	**1.11**	6.5 (0.0, 6.5)
AGF	21.2	1.04	**1.5 (1.5, 0.0)**
Proposed scheme	**20.5**	1.00	**1.5 (1.5, 0.0)**

3.2 Simulations for Walking Assistance

With its capability demonstrated above, we went on to conduct the second set of simulations by applying the proposed scheme for walking assistance. Fig. 10 shows the two scenes for simulations, the crossing and straight corridors commonly seen within a building. Eight pedestrians were arranged to walk in a steady flow. The user's applied force was assumed to be in a triangle-like waveform with a 2:7 up-down slope and a period of 2.5 seconds following the empirical evidence from our experiments. By responding to the applied force, the proposed scheme should govern the i-Go to assist him/her to move from the starting point to reach the goal without colliding with passing pedestrians.

Fig. 11 shows the resulting robot and pedestrian trajectories for the crossing-corridor simulations, where the time was identified on the right side of the robot, and Fig. 12 illustrates the corresponding state variables. From Fig. 11, the i-Go successfully accompanied the user to pass through the crowd, while several sharp turns and sudden stops occurred during the process, which would solicit the proposed scheme to respond with the inhibitory forces. As shown in Fig. 12(a), two types of inhibitory forces (the red line) were generated, which were derived according to Eq. (8) in Sec. 2.5, one (T-type) for assisting the i-Go to make the turning more smoothly, and the other (S-type) to prevent collision with the pedestrians via a larger opposing force. By taking a closer look, at 1.2, 3.7 and also 6.7 seconds, the scheme initiated three consecutive turns to deviate from the pedestrian in front; consequently, the T-typed inhibitory force, indicated by the peaks, was generated to alleviate the pushing effect due to user's applied force (the blue line), thus resulting in smoother turning. While from 11.5 to 13.7 seconds, the scene became too crowded for turning, the scheme thus resorted to the S-typed inhibitory force, indicated by the peaks, to make several temporary stops. Fig. 12(a) also shows the user's applied force in the triangle-like waveform (the blue line) and Fig. 12(b) corresponds to driving torque imposed on the i-Go generated by the proposed scheme, and Figs. 12(c) and (d) are the resultant linear and angular velocities, respectively, which exhibited smooth variations. As for the simulations in the straight-corridor environment, it also yielded similar performance, as demonstrated by the robot and pedestrian trajectories shown in Fig. 13. With successful execution of this set of simulations, the proposed navigation scheme was ready for the following experiments in the real world.

(a) Crossing corridor

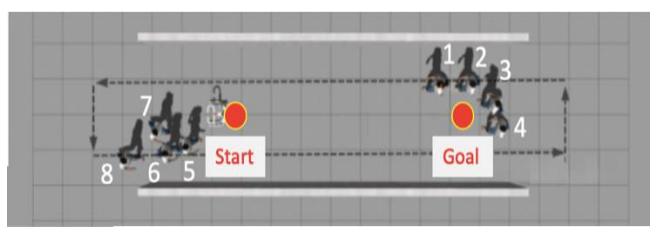

(b) Straight corridor

Fig. 10. Simulation scenes for walking assistance: (a) crossing and (b) straight corridor.

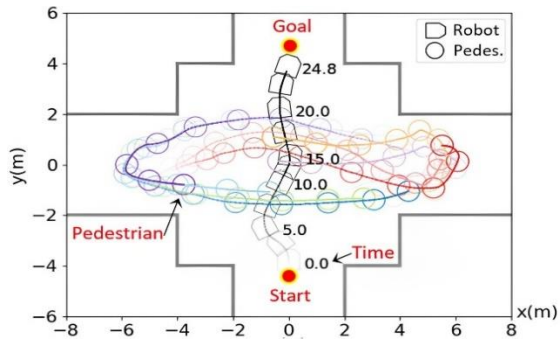

Fig. 11. The robot and pedestrians' trajectories for the crossing-corridor simulations.

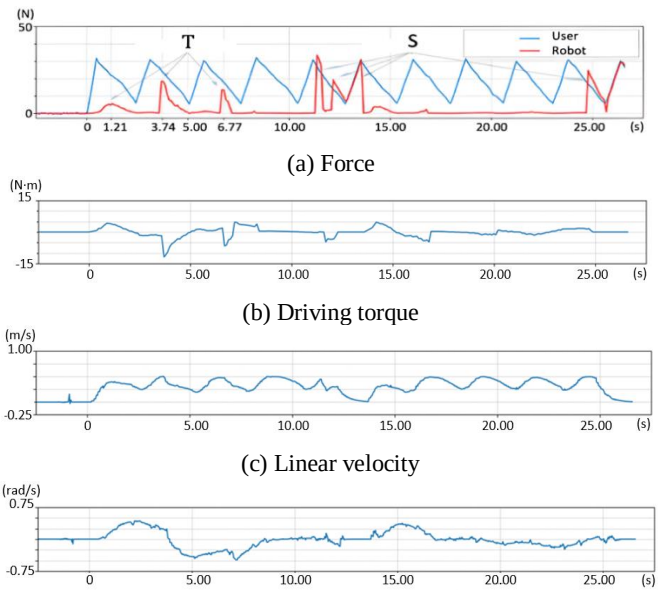

(a) Force

(b) Driving torque

(c) Linear velocity

(d) Angular velocity

Fig. 12. Corresponding state variables: (a) force, (b) driving torque, and (c) and (d) linear and angular velocities.

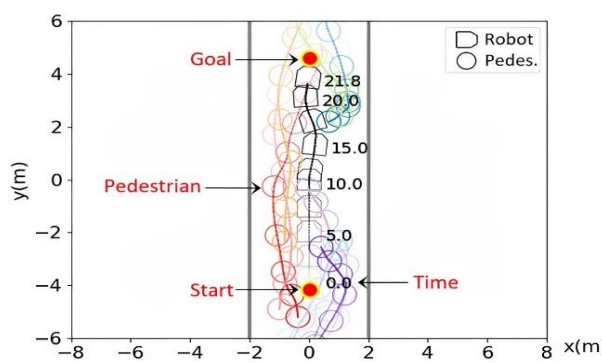

Fig. 13. The robot and pedestrians' trajectories for the straight-corridor simulations.

3.3 Field Study at Campus Cafeteria

We conducted the field study at our campus cafeteria during rush hour. Fig. 14 shows its map generated by the SLAM equipped on the i-Go through an exploration of the entire area in advance, and also the desired path intended for navigation. When facing a crowded environment with social norms to abide by, the two major actions often taken by the proposed scheme were sharp turn smoothing as well as waiting and following, as shown in Figs. 15(a) and (b), respectively. Fig. 16 shows the corresponding state variables of the i-Go. In Fig. 16(a), at 14.5 seconds, the i-Go sensed a potential collision threat, which triggered the scheme to generate a large opposing force to stop. Later at 30.5 seconds, in response to the appearance of a crowd, the scheme came up with a path of a large curvature for detouring, which should lead to sharp turning. Consequently, at 33.8 and 36.4 seconds, two inhibitory forces were generated to smooth the turning. The i-Go went on to pass tables and chairs in the seating area and finally reached the goal, during which the T- and S-typed inhibitory forces were summoned for assistance at around 50 and 59 seconds, respectively. Fig. 16(a) shows the user's applied force and Fig. 16(b) the corresponding driving torque imposed on the i-Go, and Figs. 16(c) and (d) the resultant linear and angular velocities. In summary, the experimental results have demonstrated the effectiveness of the proposed socially aware navigation scheme when applied to crowded public environments. Note: the connection to the video that shows the demonstration for this field study and the simulation for autonomous navigation can be found at https://youtu.be/XX00RrCC61g.

Regarding the computational aspects, the execution time for each module of the proposed scheme was analyzed during the field study. The visual information was captured by the 2D camera at 30 Hz and the 2D Lidar at 11 Hz fixed rates. The pedestrian tracker module processed the sensor data and output tracking information at approximately 4.7 Hz, which included pedestrian detection using YOLOv4_tiny (averaging 158 ms), point cloud clustering via DBSCAN (approximately 32 ms), and trajectory estimation through AB3DMOT (around 43 ms). The personal space generation module, which also operated at 4.7 Hz, took about 42 ms to create cost maps for social awareness. The trajectory planning module computed socially compliant paths at 3.8 Hz, with the A* algorithm requiring roughly 97 ms per iteration. Finally, the passive control module executed path-following control at a fixed rate of 10 Hz, consuming approximately 8 ms per control cycle. The total processing time for a complete navigation cycle averaged around 380 ms, which proved sufficient for real-time operation in the crowded cafeteria environment, while also demonstrated its excellence in time efficiency.

Currently, only a small number of subjects have participated in this campus-cafeteria field study. Although most of them reported that the walking-assist robot provided timely assistance during the process, especially when turning, in the next stage of the study, we plan to conduct a more thorough evaluation of system performance. More subjects will be invited for experiments, along with a questionnaire survey to collect subjects' feedback, so that meaningful statistical analysis can be achieved. The questionnaire will be designed according to system usability scale (SUS), which is widely used for evaluating human-machine interaction [26] and has been used in our previous research [10].

Fig. 14. Cafeteria map and desired path for navigation.

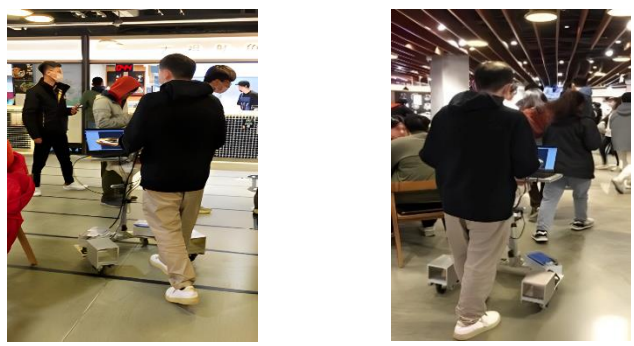

(a) Sharp turn smoothing (b) Waiting and following

Fig. 15. Two actions taken by the proposed scheme during navigation: (a) sharp turn smoothing and (b) waiting and following.

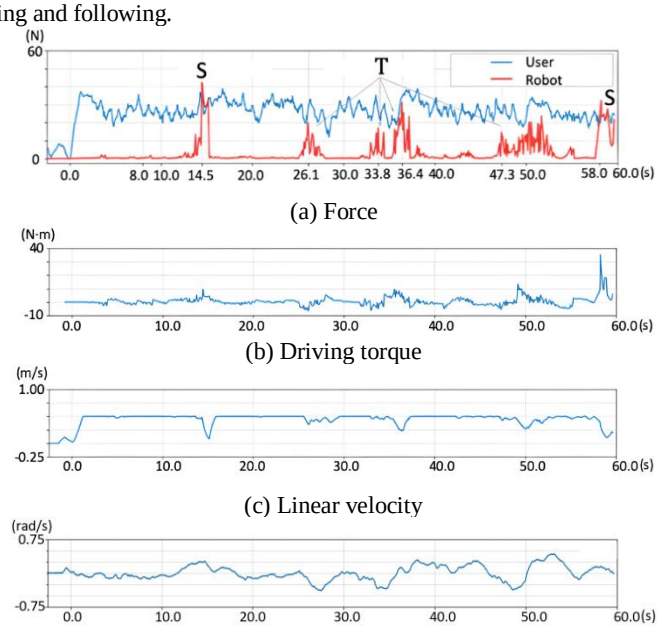

(a) Force

(b) Driving torque

(c) Linear velocity

(d) Angular velocity

Fig. 16. State variables for the i-Go during navigation: (a) force, (b) driving torque, and (c) and (d) linear and angular velocities. In (a), T and S stand for the type of inhibitory forces.

3.4 Discussions on Extensions

To extend its applications to diverse real-world environments, such as malls, parks, or hospitals, firstly, we need to check whether the proposed scheme can meet their specific requirements. In our following study, it will start with the hostipal, as the walking-assist robot suits the purpose. Compared to that of the campus cafeteria, the hospital environment poses different kinds of challenges. It can be expected that the crowd there may include patients with crutches, sitting on the wheelchairs, or accompanied by the caregiver, along with medical staffs and others, as in the simulated scene shown in Fig. 17. Meanwhile, the corresponding social norms may also be slightly different due to a very strict safety demand and special attention paid to medical staff and patients. In response, we will proceed with new formulation of personal space to accommodate the cases of individuals (with crutches or on wheelchairs) and also people in groups, and come up with more fitting social norms. The visual system will also be enhanced to be able to distinguish the incoming persons as individual or group in real-time. With these refinements, as one of our future works, we plan to conduct experiments in the hospital-like intelligent ward at our university, which is designed specifically for testing the intelligent medical systems developed by research teams in our school.

Fig. 17. A patient on the wheelchair and two persons walking together.

4. CONCLUSIONS

In this paper, we have proposed a socially aware navigation scheme for the walking-assist type of robot. Especially, it includes a new form of personal space, which is more flexible and can be adjusted according to the requirements of various social norms. Along with a novel passive controller, their combination leads to a balance between time efficiency and user's comfort during navigation. A comparison with the state-of-the-art approaches via simulations and the experiments conducted at our campus cafeteria have demonstrated its superiority. In next phase of the research, we will continue its enhancement, so that the i-Go can achieve the final goal of providing assistance for the elderly in daily lives.

ACKNOWLEDGMENT

This work was financially supported in part by the National Science and Technology Council, Taiwan.

REFERENCES

1. M. Martins, C. Santos, A. Frizera, and R. Ceres, "A review of the functionalities of smart walkers," *Medical Engineering & Physics*, Vol. 37, 2015, pp. 917-928.
2. Y. H. Hsieh, K. Y. Young, and C. H. Ko, "Effective maneuver for passive robot walking helper based on user intention," *IEEE Transactions on Industrial Electronics*, Vol. 62, 2015, pp. 6404-6416.
3. M. Kylberg, C. Löfqvist, J. Phillips, and S. Iwarsson, "Three very old men's experiences of mobility device use over time," *Scandinavian Journal of Occupational Therapy*, Vol. 20, 2013, pp. 397-405.
4. J. Rios-Martinez, A. Spalanzani, and C. Laugier, "From proxemics theory to socially-aware navigation: a survey," *International Journal of Social Robotics*, Vol. 7, 2015, pp. 137-153.
5. C. Chen, Y. Liu, S. Kreiss, and A. Alahi, "Crowd-robot interaction: crowd-aware robot navigation with attention-based deep reinforcement learning," *IEEE International Conference on Robotics and Automation*, 2019, pp. 6015-6022.
6. M. Everett, Y. F. Chen, and J. P. How, "Motion planning among dynamic, decision-making agents with deep reinforcement learning," *IEEE/RSJ International Conference on Intelligent Robots and Systems*, 2018, pp. 3052-3059.
7. D. Mehta, G. Ferrer, and E. Olson, "Autonomous navigation in dynamic social environments using multi-policy decision making," *IEEE/RSJ International Conference on Intelligent Robots and Systems*, 2016, pp. 1190-1197.
8. G. Ferrer and A. Sanfeliu, "Behavior estimation for a complete framework for human motion prediction in crowded environments," *IEEE International Conference on Robotics and Automation*, 2014, pp. 5940-5945.
9. M. Boldrer et al., "Socially-aware reactive obstacle avoidance strategy based on limit cycle," *IEEE Robotics and Automation Letters*, Vol. 5, 2020, pp. 3251-3258.
10. K. Y. Young, S. L. Cheng, C. H. Ko, and H. W. Tsou, "Development of a comfort-based motion guidance system for a robot walking helper," *Journal of Intelligent and Robotic Systems*, Vol. 100, 2020, pp. 379-388.
11. Y. H. Hsieh, Y. C. Huang, K. Y. Young, C. H. Ko, and S. K. Agrawal, "Motion guidance for a passive robot walking helper via user's applied hand forces," *IEEE Transactions on Human-Machine Systems*, Vol. 46, 2016, pp. 869-881.
12. C. H. Ko, K. Y. Young, Y. C. Huang, and S. K. Agrawal, "Active and passive control of walk-assist robot for outdoor guidance," *IEEE/ASME Transactions on Mechatronics*, Vol. 18, 2013, pp. 1211-1220.
13. M. Andreetto et al., "Simulating passivity for robotic walkers via authority-sharing," *IEEE Robotics and Automation Letters*, Vol. 3, 2018, pp. 1306-1313.
14. M. Andreetto et al., "Combining haptic and bang-bang braking actions for passive robotic walker path following," *IEEE Transactions on Haptics*, Vol. 12, 2019, pp. 542-553.
15. A. Bochkovskiy, C. Y. Wang, and H. Liao, "Yolov4: optimal speed and accuracy of

object detection," arXiv preprint arXiv:2004.10934, 2020.
16. M. E. Yabroudi, K. Awedat, R. C. Chabaan, O. Abudayyeh, and I. Abdel-Qader, "Adaptive DBSCAN lidar point cloud clustering for autonomous driving applications," *IEEE International Conference on Electro Information Technology*, 2022, pp. 221-224.
17. S. Chopra, G. Notarstefano, M. Rice, and M. Egerstedt, "A distributed version of the Hungarian method for multirobot assignment," *IEEE Transactions on Robotics*, Vol. 33, 2017, pp. 932-947.
18. X. Weng, J. Wang, D. Held, and K. Kitani, "3D multi-object tracking: a baseline and new evaluation metrics," *IEEE/RSJ International Conference on Intelligent Robots and Systems*, 2020, pp. 10359-10366.
19. D. Chugo et al., "A dynamic personal space of a pedestrian for a personal mobility vehicle," *IEEE International Conference on Cognitive Infocommunications*, 2013, pp. 223-228.
20. M. R. Batista, D. G. Macharet, and R. A. F. Romero, "Socially acceptable navigation of people with multi-robot teams," *Journal of Intelligent and Robotic Systems*, Vol. 98, 2020, pp. 481-510.
21. M. Missura and M. Bennewitz, "Predictive collision avoidance for the dynamic window approach," *International Conference on Robotics and Automation*, 2019, pp. 8620-8626.
22. H. Yang, X. Xu, and J. Hong, "Automatic parking path planning of tracked vehicle based on improved A* and DWA algorithms," *IEEE Transactions on Transportation Electrification*, Vol. 9, 2022, pp. 283-292.
23. "Pedsim_ros," 2022. Available: https://github.com/srl-freiburg/pedsim_ros.
24. B. Anvari and H. A. Wurdemann, "Modelling social interaction between humans and service robots in large public spaces," *IEEE/RSJ International Conference on Intelligent Robots and* Systems, 2020, pp. 11189-11196.
25. J. V. D. Berg, S. J. Guy, M. Lin, and D. Manocha, "Reciprocal n-body collision avoidance," *Robotics Research*, Vol. 70, 2011, pp. 3-19.
26. J. Brooke, "SUS - A quick and dirty usability scale," *Usability Evaluation in Industry*, Vol. 189, 1996, pp. 189-194.

Shih-Hsing Liu (劉士興) received his B.S. degree in electronic and computer engineering from the National Taiwan University of Science and Technology, Taipei, Taiwan, in 2018, and subsequently received his M.S. degree in electrical control engineering from National Yang Ming Chiao Tung University, Hsinchu, Taiwan, in 2021. His research interests include mobile robots, human machine interaction, and embedded systems.

Chien-Yu Su (蘇建宇) received the B.S. degree in electrical engineering from National Taipei University, New Taipei City, Taiwan, in 2018. He is currently pursuing the Ph.D. degree in electrical and computer engineering at National Yang Ming Chiao Tung University, Hsinchu, Taiwan. In 2018, he received the excellent paper award at IEEE International Conference on System Science and Engineering. His research interests include mobile robot manipulator, human machine interaction, assistive robot, and machine learning.

Chun-Hsu Ko (柯春旭) received the M.S. degree in power mechanical engineering from National Tsing Hua University, Hsinchu, Taiwan, in 1991, and the Ph.D. degree in electrical control engineering from National Yang Ming Chiao Tung University, Hsinchu, Taiwan, in 2003. From 1994 to 1998, he was with the Industrial Technology Research Institute, Hsinchu, Taiwan, as an Associate Researcher. He is currently a Professor in the department of Electrical Engineering, I-Shou University, Kaohsiung, Taiwan. His research interests include robot control, robot walking helper, and optimization.

Kuu-young Young (楊谷洋) (M'86–SM'04) was born in Kaohsiung, Taiwan, 1961. He received his B.S. degree in electrical engineering from National Taiwan University, Taiwan, in 1983, and M.S. and Ph.D. degrees in electrical engineering from Northwestern University, Evanston, IL, U.S.A., in 1987 and 1990, respectively. Since 1990, he has been with the department of Electrical Engineering at National Yang Ming Chiao Tung University, Hsinchu, Taiwan, where he is currently a Professor. He served as the chairman of the department from 2003 to 2006, and the associate dean of Electrical and Computer Engineering College, NYCU, from 2007 to 2010 and also 2014 to 2015. His research interests include robot compliance control, robot learning control, robot calibration and path planning, teleoperation, and assistive robot.

Socially Aware Navigation for a Walking-Assist Robot in a Pedestrian-Rich Environment

CHIEN-YU SU[1], SHIH-HSING LIU[1], CHUN-HSU KO[2] AND KUU-YOUNG YOUNG[1,+]
[1]*Department of Electrical Engineering*
National Yang Ming Chiao Tung University
Hsinchu, 300 Taiwan
[2]*Department of Electrical Engineering*
I-Shou University
Kaohsiung, 840 Taiwan.
**Correspondence: kyoung@nycu.edu.tw; Tel.: +886-3-5712121-54366*

As society continues to age, more elderly people experience mobility difficulties. With the walking-assist robot deemed to be helpful for their motion guidance and physical support, in this paper, we further extend its application from a home or nursing house, which may be less challenging, to more crowded environments in our daily lives. Consequently, it demands a path planner that can efficiently deal with moving pedestrians, and also be socially aware. By taking into account the comfort of both the user and pedestrians, the concept of personal space is introduced, which is in accordance with the social norms, such as walking on the left or right, not crossing in front of others, and following instead of passing a group. Furthermore, because the passive type of walking-assist robot was adopted for safety concerns, which relies mainly on the user's applied force to move, the corresponding passive control strategy is developed to realize the proposed navigation scheme. Extensive simulations and then a field study on our campus cafeteria are conducted for demonstration.

Keywords: socially aware navigation, walking-assist robot, personal space, passive control

1. INTRODUCTION

Owing to an aging society, a growing number of people suffer from mobility problems, thus soliciting the development of various kinds of walking aids [1]. Among them, the walking-assist robot is favored for being able to entice exercise, when the elders can still walk, in addition to its support for balance and motion guidance [2]. However, its current application is limited to a less challenging home or nursing house environment, as it is not that effective when interacting with a larger number of incoming persons. Motivated by it, in this paper, we propose equipping the walking-assist robot with a novel navigation scheme, so that it can be applied to a general public space, which may in turn encourage the elderly for more social engagement.

The proposed navigation scheme mainly consists of a path planner that is able to derive a feasible path among the moving pedestrians in a socially aware manner, and a control strategy capable of governing the robot to follow that path. Including social norms in path planning should benefit robot-human interaction, which is especially desirable for the assistive types of robots. Kylberg et al. pointed out that even if robots possess a highly ef-

fective collision avoidance ability, the absence of socially reassuring cues in their interactions could impact human comfort [3]. Rios-Martinez also mentioned that adherence to social customs can let the coexistence of humans and robots be more natural [4]. Meanwhile, the demand for social compliance will certainly complicate this already highly challenging task of searching for a collision-free path in a crowded space.

Previous research on socially compliant navigation has primarily focused on mobile robots, with limited applications to walking-assist robots. Nevertheless, these studies have provided valuable insights into how walking-assist robots can handle social interaction. Chen et al. proposed applying deep reinforcement learning to derive collision-free paths by analyzing the future states of nearby pedestrians; however, their method requires high computational costs, posing certain limitations for applications demanding real-time performance [5]. Everett et al. employed deep learning frameworks to train collision avoidance algorithms in multi-pedestrian environments without assuming specific behavioral rules, while this approach may generate unnatural navigation trajectories when encountering new scenarios [6]. Mehta et al. proposed a navigation scheme based on multi-policy decision-making for dynamic, unstructured environments, but it demands substantial computational resources [7]. Ferrer and Sanfeliu developed a human behavior estimator based on the social force model for environments with dynamic crowds and moving obstacles, while limitations persist when handling highly crowded scenarios [8]. Boldrer et al. combined the potential field method with limit cycles to guide robots in avoiding pedestrians' personal space, but this approach is susceptible to local minima, affecting navigation stability [9].

Among these researches, although learning approaches excel in adapting to social norms, their high computational costs and scene dependency limit their feasibility in real-time applications. In contrast, model-driven approaches offer higher computational efficiency, making them more suitable for walking-assist robots operating in crowded environments. In this study, we opt for a model-based approach, combining it with flexible personal space modeling, starting from basic types of social norms to achieve an efficient navigation solution. Extending from our previous work [10], which had included spatial and visual comfort in path planning in a static environment for an active type of walking-assistive robot, the proposed scheme will move on to deal with dynamic obstacles, and can be applied to that of a passive type for safety concerns [11].

Relative to that of autonomous robotic vehicles, the walking-assist robot poses a different kind of challenge in its close bondage with the user, while that of the passive type further raises its own in moving the robot only via the applied force from the user, which would then trigger the brakes for steering, instead of through active guidance [12]. In previous related research, Andreetto et al. introduced an authority-sharing approach, in which the motors were deactivated as the robot followed a planned path, and activated when it deviated [13]. Later, they further enhanced the system by incorporating vibrating wristbands to notify users of deviations [14]. In responding to the challenge, we come up with a new passive control strategy to realize the path derived from the proposed socially aware path planner. The effectiveness of the proposed navigation scheme is demonstrated via a series of simulations that involve various crowd scenarios and also experiments at our

campus cafeteria during rush hour. Comparing with previous approaches, we consider the proposed scheme to have the following merits:

- A novel path planner that is able to find a socially-aware collision-free path in a crowded environment is developed. To the best of our knowledge, this is the first attempt to include social norms into path planning in a pedestrian-rich environment for the walking-assist type of robot.
- A new passive control strategy that responds well to the situations resulting from the social norms, such as sharp turns or sudden stops, is developed, so that it can govern the walking-assist robot to follow the planned path effectively and smoothly.
- The proposed scheme is well integrated to be capable of conducting a field study at our campus cafeteria, with its performance compared to the state-of-the-art approaches via simulations.

The rest of this paper is organized as follows: Sec. 2 describes the proposed navigation system, including the description of the employed walking-assist robot, and the modules of pedestrian tracking, personal space generation, trajectory planning, and passive control. Simulations and experiments conducted in the campus cafeteria are reported in Sec. 3. Finally, concluding remarks are given in Sec. 4.

2. PROPOSED NAVIGATION SYSTEM

Fig. 1 shows a conceptual diagram of the proposed navigation scheme, including the modules for pedestrian tracking, personal space generation, trajectory planning, and passive control. The walking-assist robot employed in this study is named as i-Go, which is an advanced version of that previously developed in our laboratory [12], described in Section 2.1. In Fig. 1, as the user maneuvers the walking-assistive robot to enter a crowded environment for daily activities, sensors, such as a camera and Lidar, will be activated to collect information of the incoming pedestrians and others, which will then be forwarded to the pedestrian tracker for analysis, described in Section 2.2. With the environmental status available, the personal space generator will then determine the personal space adhering to social norms that corresponds to each individual, described in Section 2.3, and also build a cost map for the path planner to derive a socially compliant path, described in Section 2.4. In turn, the passive controller will be employed to ensure successful execution of the planned path via salient management of the demands from both the user and social norms, described in Section 2.5.

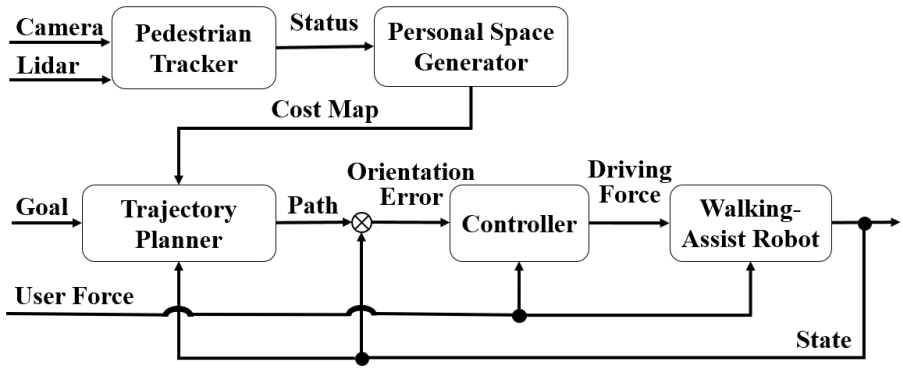

Fig. 1. A conceptual diagram for the proposed navigation scheme.

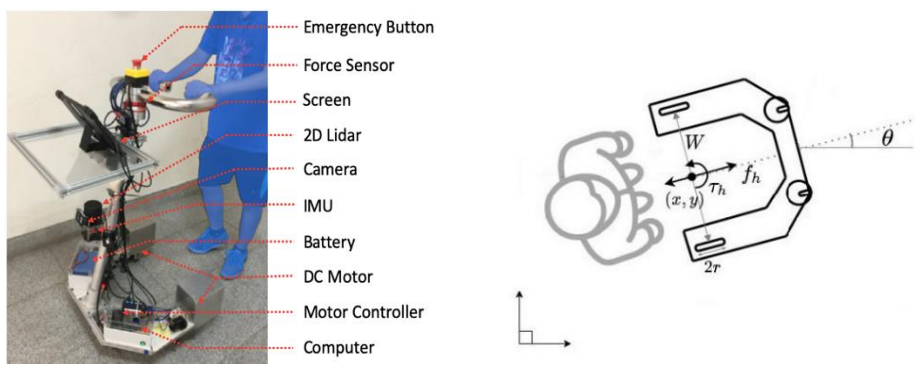

(a) Outlook (b) Chassis

Fig. 2. The walking-assist robot i-Go and its chassis: (a) outlook and (b) chassis.

2.1 Walking-Assist Robot

Fig. 2(a) shows the outlook of the walking-assist robot, named as i-Go, which is at a height of 1.1 m, with left and right auxiliary wheels attached with corresponding DC motors. Several sensors are equipped, including a six-axis force sensor (WACOH) for user's applied force measurement, 2D camera (Logitech) for pedestrian detection, 2D Lidar (YDLIDAR) for obstacle detection and robot positioning, and IMU (Sparkfun) also for robot positioning. The Jetson Xavier NX embedded computer (NVIDIA) was adopted as the computing platform, and an emergency stop switch was installed for safety considerations. During task execution, the user first applies force to maneuver the i-Go, which is measured by the force sensor. The measured force, along with the visual information of the pedestrians and obstacles, are then forwarded to the proposed scheme to derive a socially compliant path for navigation, which is further processed by the passive controller to generate proper braking torques for motion assistance.

Fig. 2(b) shows the chassis of i-Go with a rotational center (x, y) and a heading angle θ in Cartesian coordinates. Assuming the walking-assist robot moves on a flat surface without wheel slip, we can obtain [11]

$$\dot{q} = \begin{bmatrix} cos\theta & 0 \\ sin\theta & 0 \\ 0 & 1 \end{bmatrix} V \tag{1}$$

where $q = [x, y, \theta]^T$, V is the vector of the speed v and angular speed ω, i.e., $V = [v, \omega]^T$. By further assuming the walking-assist robot is symmetric, its dynamic equation can be derived as

$$\dot{V} + \begin{bmatrix} \frac{D_{xy}}{m} & 0 \\ 0 & \frac{D_\theta}{J} \end{bmatrix} V = \mathbf{A}\tau_m + \begin{bmatrix} \frac{1}{m} & 0 \\ 0 & \frac{1}{J} \end{bmatrix} F_h \tag{2}$$

with

$$\mathbf{A} = \begin{bmatrix} \frac{1}{mr} & \frac{1}{mr} \\ \frac{W}{2Jr} & -\frac{W}{2Jr} \end{bmatrix},\ \tau_m = \begin{bmatrix} \tau_r \\ \tau_l \end{bmatrix},\ F_h = \begin{bmatrix} f_h \\ \tau_h \end{bmatrix} \tag{3}$$

where f_h and τ_h stand for user's applied force and torque, respectively, τ_r and τ_l for the torque generated by right and left wheels, respectively, $D_{xy} = 45.0\ (\mathrm{N \cdot s/m})$ and $D_\theta = 20.0\ (\mathrm{N \cdot m \cdot s/rad})$ as the damping parameters, $r = 0.0625\ \mathrm{m}$, $W = 0.6\ \mathrm{m}$, $m = 30\ \mathrm{kg}$, and $J = 10.0\ (\mathrm{kg \cdot m^2})$ as the wheel radius, distance between the rear wheels, mass of the robot, and its moment of inertia, respectively. This dynamic equation will then be utilized to derive the passive control strategy in Sec. 2.5.

2.2 Pedestrian Tracking

The pedestrian tracker is used to acquire the status of the pedestrians via close monitoring of their movements in a crowded environment, intended for the following personal space generation and path planning. It thus needs to be able to differentiate the pedestrians from the static obstacles, and also determine their directions relative to the robot. Fig. 3 shows its process. The images of the pedestrians obtained by the 2D camera are first bounded by using the Yolov4_tiny neural network [15], which are assigned with directional vectors from the robot to the *m* pedestrians, denoted as $\vec{U}_{\mathrm{d}} = [\vec{u}_{\mathrm{d}}^{1}, \vec{u}_{\mathrm{d}}^{2}, \cdots, \vec{u}_{\mathrm{d}}^{m}]$. Meanwhile, the point clouds obtained from the 2D Lidar are clustered into groups by using the DBSCAN (density-based spatial clustering of applications with noise algorithm) [16], which are assigned with vectors that identify the distances and directions of each Lidar cluster (including obstacles and pedestrians), denoted as $\vec{U}_{\mathrm{s}} = [\vec{u}_{\mathrm{s}}^{1}, \vec{u}_{\mathrm{s}}^{2}, \cdots, \vec{u}_{\mathrm{s}}^{n}]$. While both $\vec{U}_{\mathrm{d}}$ and $\vec{U}_{\mathrm{s}}$ are available, the Hungarian algorithm [17], commonly used for solving assignment problems, is then employed to accurately allocate the cluster to their respective pedestrian with the coordinates $\boldsymbol{C}$. As the pedestrians may be obstructed by objects or other pedestrians during the tracking process, the AB3DMOT (A Baseline for 3D Multi-Object Tracking) [18], known for its effectiveness in 3D multi-object tracking, is then used to estimate the pedestrians' positions, directions, and velocities. Finally, the state vectors of the pedestrians S_h in the global coordinate system, including their position, direction, and velocity, are derived from a series of $\boldsymbol{C}$:

$$S_h = \left[s_h^1, s_h^2, \ldots, s_h^i\right] \tag{4}$$

where $s_h^i = [x_0, y_0, \theta, v]$, denoting the state of the i^{th} pedestrian, with x_0 and y_0 representing the pedestrian's position, as θ and v stand for the direction and velocity, respectively.

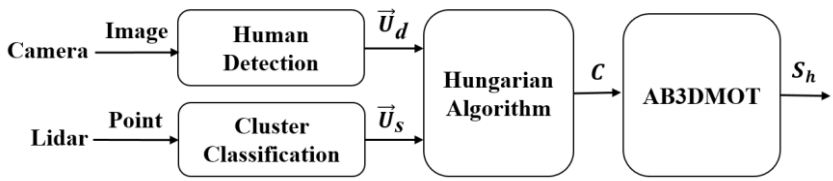

Fig. 3. The pedestrian tracking process.

2.3 Personal Space Generation

The inclusion of social awareness into path planning can be realized basically by surrounding a person with a zone as a buffer, referred to as a personal space [10]. It started with simply using a circle, as shown in Fig. 4(a) [19]. To respond to the situation that people may experience higher psychological stress when facing the incoming object, Batista et al. suggested using an asymmetric Gaussian function (AGF), so that more space should be allocated in front, as shown in Fig. 4(b) [20]. To meet the requirements for the specific social norms, in this paper, we further propose a new form of personal space, AGF-SN (asymmetric Gaussian function-social norm), that allows the Gaussian function to vary its sizes in various portions accordingly, as shown in Fig. 4(c).

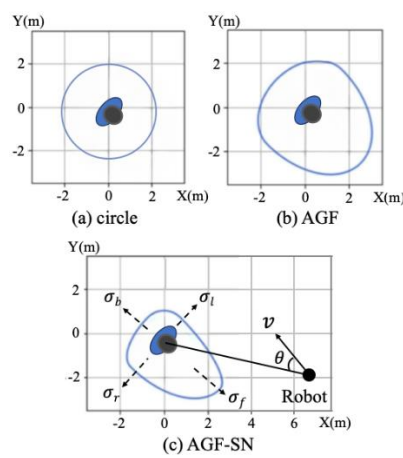

Fig. 4. Three kinds of social spaces: (a) circle, (b) AGF, and (c) AGF-SN.

(a) adhering to the walking left/right convention (b) yielding when crossing (c) following behind a group

Fig. 5. Three basic social norms (right-handed rule): (a) adhering to the walking left/right convention, (b) yielding when crossing, and (c) following behind a group.

Fig. 5 shows the three basic types of social norms selected for the robot to abide by, including adhering to the walking left/right convention, yielding when crossing, and following behind a group. In response, we propose the AGF-SN, which is designed to be able to vary its sizes in the front, back, and two sides, and also according to the approaching speeds of the pedestrians. The AGF-SN is formulated by using the asymmetric Gaussian function, but with much flexibility in its shape variation to comply with social norms. Referring to Fig. 4(c), for each point (x, y) within the personal space described by AGF-SN, the function $f_p(x, y)$ that derives its corresponding cost when facing an incoming pedestrian is formulated as

$$f_p(x, y) = e^{-(a(x-x_0)^2+2b(x-x_0)(y-y_0)+c(y-y_0)^2)} \tag{5}$$

where (x_0, y_0) is the position of the pedestrian, and a, b, and c are the functions of σ_f, σ_b, σ_r, σ_l, and θ for determining its shape, size, and orientation, with θ indicating the direction of the robot relative to the pedestrian, and σ_f, σ_b, σ_r, and σ_l the variance for its front, back, right, and left direction, respectively.

To respond the social norms of adhering to the left(right) walking convention, yielding when crossing, and following behind a group, the strategy is to choose smaller σ_r (σ_l) and σ_b, so that $f_p(x, y)$ will come up with lower costs in the left(right) and back sides of the space, prompting the robot to obey these rules. The values of these parameters may also be adjusted along with the increase(decrease) of the pedestrian's movement speed. During our experiments, we set $\sigma_b = 0.3\sigma_f$, $\sigma_r = 0.6\sigma_f$, $\sigma_l = 0.3\sigma_f$, and σ_f to be 1 by assuming the average pedestrian speed to be 0.5 m/s. These parameters were suitable for our experiments under the walking-right convention, while they can be adjusted to fit different social norms and working environments.

Meanwhile, for the case that the pedestrian stands still, we let $f_p(x, y)$ become symmetric by setting $a = c$ and $b = 0$, as users' moving directions are unknown. As for static obstacles, such as walls and tables, the symmetric Gaussian function is also used, but with smaller variances for their non-human nature. By integrating all space costs, it allows for

the creation of a cost map $\mathcal{M}$, with the cost for each of its grid cells adjusted to range from 0 to 1.

2.4 Trajectory Planning

Navigating a robot in a crowded environment is very challenging, particularly with the social norms to adhere to. The learning approach, such as deep reinforcement learning, has shown its potential in dealing with complex environments, but may result in unnatural trajectories when encountering previously unseen scenarios [5-6]. The potential field approach is capable of overcoming unknown scenes through its intuitiveness, while facing the possibility of getting stuck in local minima [7]. Meanwhile, the dynamic window approach is deemed to be effective for dynamic obstacle avoidance, which is at the expense of high computational load [21].

Due to real time consideration and limited computational resources on the walking-assist robot, our design concept is first to plan a shortest path $\mathcal{P}$ to reach the goal *G* under the social norm constraint based on the cost map $\mathcal{M}$ derived in Sec. 2.2 above. The robot should follow $\mathcal{P}$, except when the incoming pedestrian(s) blocks the path within its sensing distance (set to be around 5 m). It would detour to avoid them, and then return back to $\mathcal{P}$. Following the concept, we chose a relatively simple A* algorithm [22] to plan path $\mathcal{P}$, with the cost $\mathcal{F}$ that considered social norms, derived to be

$$\mathcal{F} = G + \mathcal{H} + k \cdot I \tag{6}$$

where G stands for the cost for movement from the starting point to a specified grid cell, $\mathcal{H}$ the estimated cost from that cell to the destination, I the cost for the cell in the cost map corresponding to social norms $\mathcal{M}$ derived in Section 2.2, and k the weight.

For the situation that a pedestrian is detected to get into the way, the planner will search for a temporary goal within the range of 0°~180° at a 10° interval, which is determined by considering both its cost on map $\mathcal{M}$ and distance to goal *G*. Because the walking-assist robot is not meant to move fast, the proposed planner serves well, as demonstrated by the simulations and experiments later.

2.5 Passive Control

To ensure that the walking-assist robot can smoothly follow the planned path derived above, especially under the circumstance that sharp turns or sudden stops may occur due to compliance with social norms, a new passive controller is proposed based on that previously developed in our laboratory [11]. Fig. 6 shows the scene in which the walking-assist robot is guiding a user to follow a desired path. The proposed controller is intended to minimize both the orientation error $\tilde{\theta} = \theta - \psi$, i.e., the angle between the robot and trajectory $\mathcal{P}$, and the position error d, i.e., the shortest distance from the robot to $\mathcal{P}$. With a slow-moving robot, the orientation error should be small, so that their derivatives can be derived as

$$\dot{\tilde{\theta}} = \tilde{\omega} = \omega - \omega_d, \ \dot{d} = v \cdot \tilde{\theta} \tag{7}$$

where $\tilde{\omega}$, ω, and ω_d are the rotational velocity error, actual and desired rotational velocities, respectively, and v is the linear velocity.

To respond to possible sharp turns due to social norm adherence, we propose adding an inhibitory force f_{inh} to slow down robot's speed in a smooth manner. For this purpose, the magnitude of f_{inh} is set to be zero when there is no orientation error ($\tilde{\theta}$), and gradually increases until $\tilde{\theta}$ reaches π/4. Accordingly, as shown in Fig. 7, f_{inh} is chosen to be

$$f_{inh} = -f_h/(1 + \exp(-40|\tilde{\theta}|/\pi + 5)) \tag{8}$$

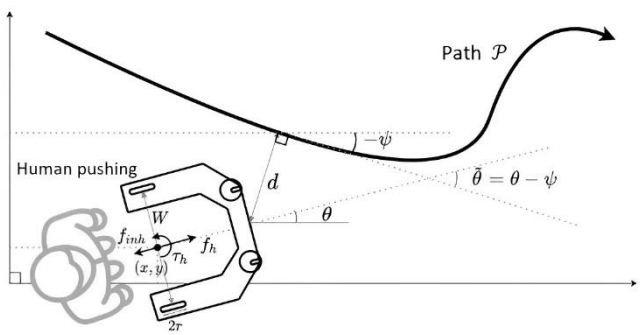

Fig. 6. The walking-assist robot is guiding a user to follow the desired path.

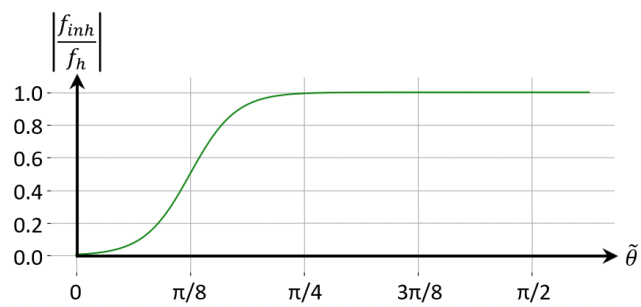

Fig. 7. Illustration for f_{inh} vs. $\tilde{\theta}$.

With f_{inh} included and considering the dynamic equation in Eq.(2), we set up the control law by choosing τ_m to be

$$\tau_m = \mathbf{A}^{-1}\begin{bmatrix} f_{inh}/m \\ \frac{D_\theta \omega}{J} - \frac{\tau_h}{J} - k_1\dot{\tilde{\theta}} - k_2\tilde{\theta} + \dot{\omega_d} \end{bmatrix} \tag{9}$$

where k_1 and k_2 represent control gains, with both greater than 0. By substituting (9) into (2), it leads to

$$\begin{bmatrix}\dot{v}\\ \dot{\omega}\end{bmatrix}+\begin{bmatrix}\frac{D_{xy}}{m} & 0\\ 0 & \frac{D_\theta}{J}\end{bmatrix}\begin{bmatrix}v\\ \omega\end{bmatrix}=\begin{bmatrix}\frac{f_{inh}}{m}\\ \frac{D_\theta\omega}{J}-\frac{\tau_h}{J}-k_1\dot{\tilde{\theta}}-k_2\tilde{\theta}+(\dot{\omega}-\dot{\hat{\omega}})\end{bmatrix}+\begin{bmatrix}\frac{1}{m} & 0\\ 0 & \frac{1}{J}\end{bmatrix}\begin{bmatrix}f_h\\ \tau_h\end{bmatrix} \quad (10)$$

After rearrangement, we can obtain

$$\ddot{\tilde{\theta}}+k_1\dot{\tilde{\theta}}+k_2\tilde{\theta}=0 \quad (11)$$

With k_1 and k_2 positive, orientation error $\tilde{\theta}$ should converges to zero. And, via Eq.(7), we can also obtain that $\dot{d}=v\cdot\tilde{\theta}$ converges to zero. Since the planned path starts at the robot's current position, with the initial position error being zero, the position error d should converge to a small value, demonstrating the stability of the proposed control law.

Here, we propose another controller, which is intended for robot autonomous navigation. The reason is that we intend to compare the performance of the proposed navigation scheme with those related state-of-the-art methods, while most of them have been applied to autonomous robotic vehicles. Our strategy is to let the walking-assist robot behave like an autonomous mobile one, i.e., it is without the governance from the user. Consequently, by removing user's applied force F_h, the dynamic equation in Eq.(5) becomes

$$\dot{V}+\begin{bmatrix}\frac{D_{xy}}{m} & 0\\ 0 & \frac{D_\theta}{J}\end{bmatrix}V=\mathbf{A}\tau_m \quad (12)$$

By selecting v_{pref} as the desired velocity for this mobile robot and applying the similar concept on designing f_{inh} in Eq.(8) for smoothing the impact from sharp turning, we come up with a corresponding control law by choosing τ_m to be

$$\tau_m=\mathbf{A}^{-1}\begin{bmatrix}\frac{D_{xy}v}{m}-k_1\left(v-v_{pref}\right)-\frac{v_{pref}}{1+\exp(-40|\tilde{\theta}|/\pi+5)}\\ \frac{D_\theta\omega}{J}-k_1\dot{\tilde{\theta}}-k_2\tilde{\theta}+\dot{\omega}_d\end{bmatrix} \quad (13)$$

where k_1 and k_2 are set to be the same as that for the walking assist robot. The stability of this controller can be proved following the similar procedure above.

3. SIMULATIONS AND EXPERIMENTS

We conducted a series of simulations and experiments based on using the i-Go to evaluate the performance of the proposed navigation scheme, including a comparison with the state-of-the-art methods and a field study at our campus cafeteria during rush hour. For simulations, we first used Solidworks to build a proportional model of the i-Go, shown in Fig. 8, including all components and sensors, and then Gazebo 9 for rendering the corresponding functions, such as sensing and control, in addition to the working environment.

For pedestrian emulation, the Pedsim_ROS library [23] was utilized to furnish each pedestrian with a human-like behavior [24]. We took into account the uncertainty of information processing, sensing noise, etc., and also considered the situations that might lead to misjudgment, such as the case that pedestrians were occluded by others, to make the simulated environment more realistic.

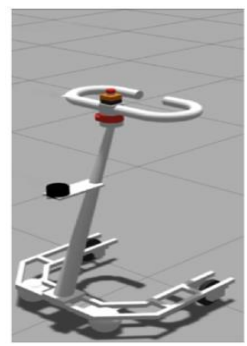

Fig. 8. The virtual walking-assistive robot used in the simulations.

3.1 Comparison with State-of-the-Art Methods

The first set of simulations were intended to compare the performance of the proposed navigation scheme with that of the state-of-the-art methods, including the Optimal Reciprocal Collision Avoidance (ORCA) approach based on the concept of velocity obstacle [25], and the two reinforcement learning approaches reviewed in the introduction, LM-SARL [5] and LSTM-RL [6], in addition to our previous approach on comfort-based motion guidance (CBMG) [10] and that using the asymmetric Gaussian function (AGF) to formulate personal space for social navigation [20]. Because most of the methods were developed for autonomous navigation, we let i-Go behave like an autonomous mobile robot during simulations, and adopted the control law in Eq. (13) for the proposed navigation scheme.

We developed the simulated environment to be similar to that used in [5][6], in which the pedestrians were randomly distributed on a circular path of 8 m in diameter, as shown in Fig. 9. They moved in a manner that might cross each other, and the robot needed to pass them to reach the goal on the other end. Both pedestrian and robot speeds were set to be 0.5 m per second to allow more interaction, with an angular velocity of 0.5 radian per second for the robot. A total of 200 trials were conducted and the number of pedestrians selected to be 4 and 8. The results are listed in Table 1, including the time for the robot to reach the destination, average minimum distance between pedestrians and the robot, and the number of navigation failure. Referring to Table 1, the CBMG led to a most comfortable path for the pedestrians with a largest average shortest distance between the pedestrian and robot, but it also spent the longest time to reach the destination for its conservative nature. The AGF exhibited the second-best time efficiency, that might be attributed to the introduction of the personal space. LSTM-RL had the highest failure rate, while ORCA and LM-SARL had mediocre performance. Meanwhile, the results show that the proposed scheme achieved a better balance between time efficiency and pedestrian comfort, as it

was with a more flexible personal space and a path planner was capable of locating a shorter path among the crowd.

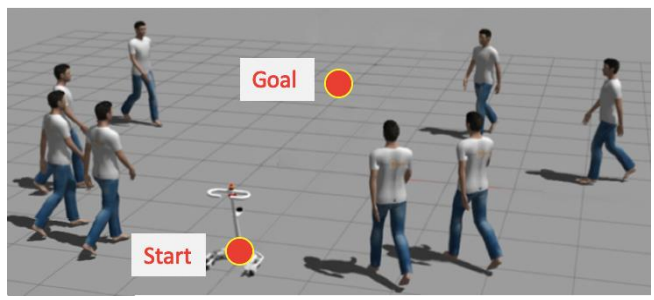

Fig. 9. Simulation scene for comparison with the state-of-the-art methods.

Table 1. Simulation results for autonomous navigation

Method	Average time (s)	Average shortest distance to pedestrian (m)	Failure (collision, timeout)
	4 pedestrians		
ORCA	20.2	1.10	2.5 (1.5, 1.0)
LM-SARL	20.2	0.99	3.5 (2.5, 1.0)
LSTM-RL	26.3	0.91	35.0 (10.5, 24.5)
CBMG	20.5	**1.20**	2.5 (0.0, 2.5)
AGF	19.7	1.07	**1.0 (1.0, 0.0)**
Proposed scheme	**19.3**	1.05	**1.0 (1.0, 0.0)**
	8 pedestrians		
ORCA	21.5	1.04	3.0 (0.5, 2.5)
LM-SARL	23.2	1.04	9.0(8.0, 1.0)
LSTM-RL	27.2	0.85	45.0 (36.5, 8.5)
CBMG	23.3	**1.11**	6.5 (0.0, 6.5)
AGF	21.2	1.04	**1.5 (1.5, 0.0)**
Proposed scheme	**20.5**	1.00	**1.5 (1.5, 0.0)**

3.2 Simulations for Walking Assistance

With its capability demonstrated above, we went on to conduct the second set of simulations by applying the proposed scheme for walking assistance. Fig. 10 shows the two scenes for simulations, the crossing and straight corridors commonly seen within a building. Eight pedestrians were arranged to walk in a steady flow. The user's applied force was assumed to be in a triangle-like waveform with a 2:7 up-down slope and a period of 2.5 seconds following the empirical evidence from our experiments. By responding to the applied force, the proposed scheme should govern the i-Go to assist him/her to move from the starting point to reach the goal without colliding with passing pedestrians.

Fig. 11 shows the resulting robot and pedestrian trajectories for the crossing-corridor simulations, where the time was identified on the right side of the robot, and Fig. 12 illustrates the corresponding state variables. From Fig. 11, the i-Go successfully accompanied the user to pass through the crowd, while several sharp turns and sudden stops occurred during the process, which would solicit the proposed scheme to respond with the inhibitory forces. As shown in Fig. 12(a), two types of inhibitory forces (the red line) were generated, which were derived according to Eq. (8) in Sec. 2.5, one (T-type) for assisting the i-Go to make the turning more smoothly, and the other (S-type) to prevent collision with the pedestrians via a larger opposing force. By taking a closer look, at 1.2, 3.7 and also 6.7 seconds, the scheme initiated three consecutive turns to deviate from the pedestrian in front; consequently, the T-typed inhibitory force, indicated by the peaks, was generated to alleviate the pushing effect due to user's applied force (the blue line), thus resulting in smoother turning. While from 11.5 to 13.7 seconds, the scene became too crowded for turning, the scheme thus resorted to the S-typed inhibitory force, indicated by the peaks, to make several temporary stops. Fig. 12(a) also shows the user's applied force in the triangle-like waveform (the blue line) and Fig. 12(b) corresponds to driving torque imposed on the i-Go generated by the proposed scheme, and Figs. 12(c) and (d) are the resultant linear and angular velocities, respectively, which exhibited smooth variations. As for the simulations in the straight-corridor environment, it also yielded similar performance, as demonstrated by the robot and pedestrian trajectories shown in Fig. 13. With successful execution of this set of simulations, the proposed navigation scheme was ready for the following experiments in the real world.

(a) Crossing corridor

(b) Straight corridor

Fig. 10. Simulation scenes for walking assistance: (a) crossing and (b) straight corridor.

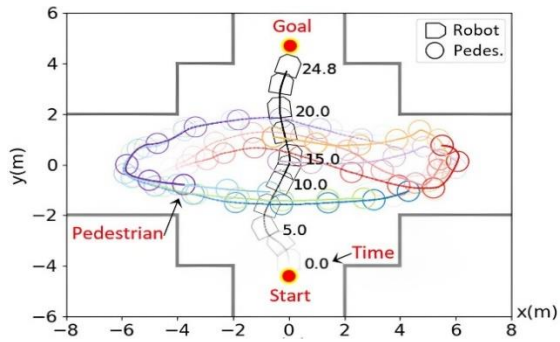

Fig. 11. The robot and pedestrians' trajectories for the crossing-corridor simulations.

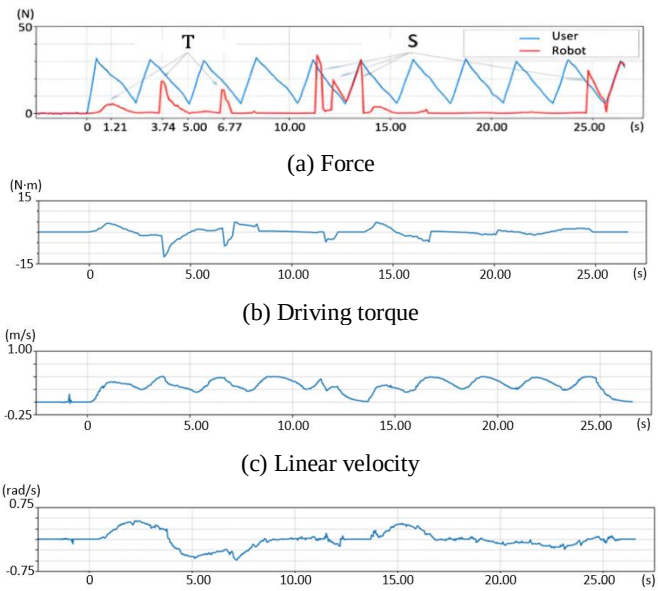

(a) Force

(b) Driving torque

(c) Linear velocity

(d) Angular velocity

Fig. 12. Corresponding state variables: (a) force, (b) driving torque, and (c) and (d) linear and angular velocities.

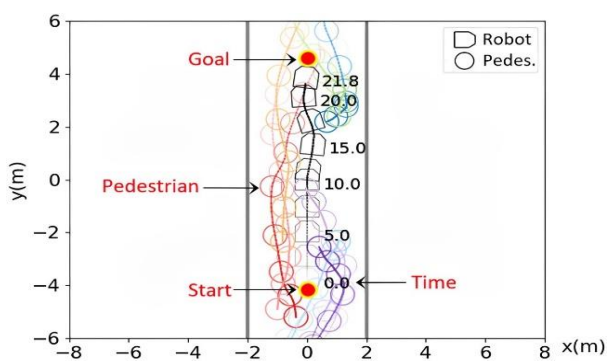

Fig. 13. The robot and pedestrians' trajectories for the straight-corridor simulations.

3.3 Field Study at Campus Cafeteria

We conducted the field study at our campus cafeteria during rush hour. Fig. 14 shows its map generated by the SLAM equipped on the i-Go through an exploration of the entire area in advance, and also the desired path intended for navigation. When facing a crowded environment with social norms to abide by, the two major actions often taken by the proposed scheme were sharp turn smoothing as well as waiting and following, as shown in Figs. 15(a) and (b), respectively. Fig. 16 shows the corresponding state variables of the i-Go. In Fig. 16(a), at 14.5 seconds, the i-Go sensed a potential collision threat, which triggered the scheme to generate a large opposing force to stop. Later at 30.5 seconds, in response to the appearance of a crowd, the scheme came up with a path of a large curvature for detouring, which should lead to sharp turning. Consequently, at 33.8 and 36.4 seconds, two inhibitory forces were generated to smooth the turning. The i-Go went on to pass tables and chairs in the seating area and finally reached the goal, during which the T- and S-typed inhibitory forces were summoned for assistance at around 50 and 59 seconds, respectively. Fig. 16(a) shows the user's applied force and Fig. 16(b) the corresponding driving torque imposed on the i-Go, and Figs. 16(c) and (d) the resultant linear and angular velocities. In summary, the experimental results have demonstrated the effectiveness of the proposed socially aware navigation scheme when applied to crowded public environments. Note: the connection to the video that shows the demonstration for this field study and the simulation for autonomous navigation can be found at https://youtu.be/XX00RrCC61g.

Regarding the computational aspects, the execution time for each module of the proposed scheme was analyzed during the field study. The visual information was captured by the 2D camera at 30 Hz and the 2D Lidar at 11 Hz fixed rates. The pedestrian tracker module processed the sensor data and output tracking information at approximately 4.7 Hz, which included pedestrian detection using YOLOv4_tiny (averaging 158 ms), point cloud clustering via DBSCAN (approximately 32 ms), and trajectory estimation through AB3DMOT (around 43 ms). The personal space generation module, which also operated at 4.7 Hz, took about 42 ms to create cost maps for social awareness. The trajectory planning module computed socially compliant paths at 3.8 Hz, with the A* algorithm requiring roughly 97 ms per iteration. Finally, the passive control module executed path-following control at a fixed rate of 10 Hz, consuming approximately 8 ms per control cycle. The total processing time for a complete navigation cycle averaged around 380 ms, which proved sufficient for real-time operation in the crowded cafeteria environment, while also demonstrated its excellence in time efficiency.

Currently, only a small number of subjects have participated in this campus-cafeteria field study. Although most of them reported that the walking-assist robot provided timely assistance during the process, especially when turning, in the next stage of the study, we plan to conduct a more thorough evaluation of system performance. More subjects will be invited for experiments, along with a questionnaire survey to collect subjects' feedback, so that meaningful statistical analysis can be achieved. The questionnaire will be designed according to system usability scale (SUS), which is widely used for evaluating human-machine interaction [26] and has been used in our previous research [10].

Fig. 14. Cafeteria map and desired path for navigation.

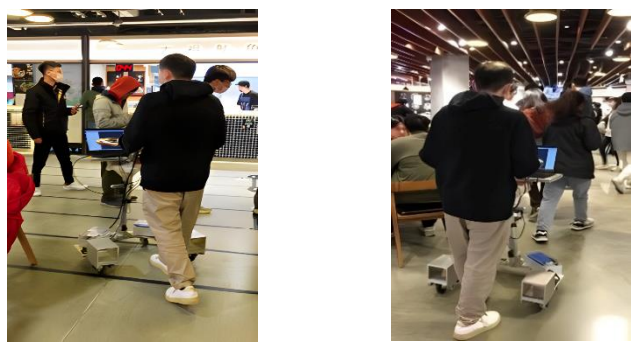

(a) Sharp turn smoothing (b) Waiting and following

Fig. 15. Two actions taken by the proposed scheme during navigation: (a) sharp turn smoothing and (b) waiting and following.

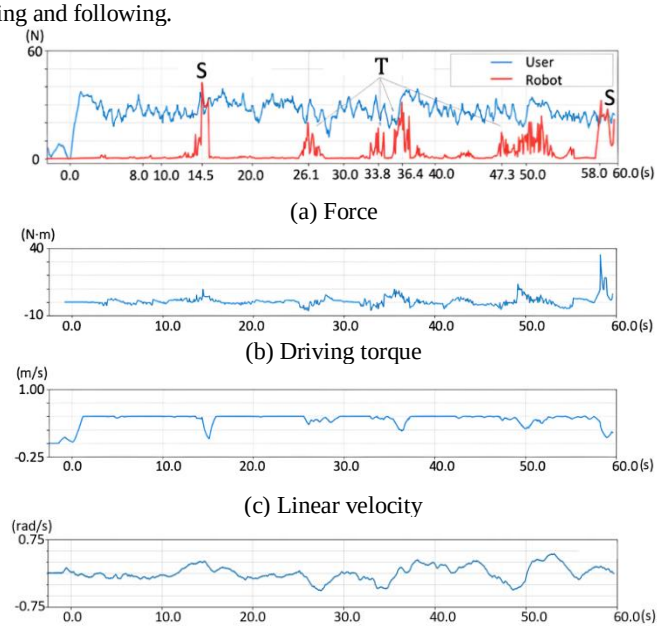

(a) Force

(b) Driving torque

(c) Linear velocity

(d) Angular velocity

Fig. 16. State variables for the i-Go during navigation: (a) force, (b) driving torque, and (c) and (d) linear and angular velocities. In (a), T and S stand for the type of inhibitory forces.

3.4 Discussions on Extensions

To extend its applications to diverse real-world environments, such as malls, parks, or hospitals, firstly, we need to check whether the proposed scheme can meet their specific requirements. In our following study, it will start with the hostipal, as the walking-assist robot suits the purpose. Compared to that of the campus cafeteria, the hospital environment poses different kinds of challenges. It can be expected that the crowd there may include patients with crutches, sitting on the wheelchairs, or accompanied by the caregiver, along with medical staffs and others, as in the simulated scene shown in Fig. 17. Meanwhile, the corresponding social norms may also be slightly different due to a very strict safety demand and special attention paid to medical staff and patients. In response, we will proceed with new formulation of personal space to accommodate the cases of individuals (with crutches or on wheelchairs) and also people in groups, and come up with more fitting social norms. The visual system will also be enhanced to be able to distinguish the incoming persons as individual or group in real-time. With these refinements, as one of our future works, we plan to conduct experiments in the hospital-like intelligent ward at our university, which is designed specifically for testing the intelligent medical systems developed by research teams in our school.

Fig. 17. A patient on the wheelchair and two persons walking together.

4. CONCLUSIONS

In this paper, we have proposed a socially aware navigation scheme for the walking-assist type of robot. Especially, it includes a new form of personal space, which is more flexible and can be adjusted according to the requirements of various social norms. Along with a novel passive controller, their combination leads to a balance between time efficiency and user's comfort during navigation. A comparison with the state-of-the-art approaches via simulations and the experiments conducted at our campus cafeteria have demonstrated its superiority. In next phase of the research, we will continue its enhancement, so that the i-Go can achieve the final goal of providing assistance for the elderly in daily lives.

ACKNOWLEDGMENT

This work was financially supported in part by the National Science and Technology Council, Taiwan.

REFERENCES

1. M. Martins, C. Santos, A. Frizera, and R. Ceres, "A review of the functionalities of smart walkers," *Medical Engineering & Physics*, Vol. 37, 2015, pp. 917-928.
2. Y. H. Hsieh, K. Y. Young, and C. H. Ko, "Effective maneuver for passive robot walking helper based on user intention," *IEEE Transactions on Industrial Electronics*, Vol. 62, 2015, pp. 6404-6416.
3. M. Kylberg, C. Löfqvist, J. Phillips, and S. Iwarsson, "Three very old men's experiences of mobility device use over time," *Scandinavian Journal of Occupational Therapy*, Vol. 20, 2013, pp. 397-405.
4. J. Rios-Martinez, A. Spalanzani, and C. Laugier, "From proxemics theory to socially-aware navigation: a survey," *International Journal of Social Robotics*, Vol. 7, 2015, pp. 137-153.
5. C. Chen, Y. Liu, S. Kreiss, and A. Alahi, "Crowd-robot interaction: crowd-aware robot navigation with attention-based deep reinforcement learning," *IEEE International Conference on Robotics and Automation*, 2019, pp. 6015-6022.
6. M. Everett, Y. F. Chen, and J. P. How, "Motion planning among dynamic, decision-making agents with deep reinforcement learning," *IEEE/RSJ International Conference on Intelligent Robots and Systems*, 2018, pp. 3052-3059.
7. D. Mehta, G. Ferrer, and E. Olson, "Autonomous navigation in dynamic social environments using multi-policy decision making," *IEEE/RSJ International Conference on Intelligent Robots and Systems*, 2016, pp. 1190-1197.
8. G. Ferrer and A. Sanfeliu, "Behavior estimation for a complete framework for human motion prediction in crowded environments," *IEEE International Conference on Robotics and Automation*, 2014, pp. 5940-5945.
9. M. Boldrer et al., "Socially-aware reactive obstacle avoidance strategy based on limit cycle," *IEEE Robotics and Automation Letters*, Vol. 5, 2020, pp. 3251-3258.
10. K. Y. Young, S. L. Cheng, C. H. Ko, and H. W. Tsou, "Development of a comfort-based motion guidance system for a robot walking helper," *Journal of Intelligent and Robotic Systems*, Vol. 100, 2020, pp. 379-388.
11. Y. H. Hsieh, Y. C. Huang, K. Y. Young, C. H. Ko, and S. K. Agrawal, "Motion guidance for a passive robot walking helper via user's applied hand forces," *IEEE Transactions on Human-Machine Systems*, Vol. 46, 2016, pp. 869-881.
12. C. H. Ko, K. Y. Young, Y. C. Huang, and S. K. Agrawal, "Active and passive control of walk-assist robot for outdoor guidance," *IEEE/ASME Transactions on Mechatronics*, Vol. 18, 2013, pp. 1211-1220.
13. M. Andreetto et al., "Simulating passivity for robotic walkers via authority-sharing," *IEEE Robotics and Automation Letters*, Vol. 3, 2018, pp. 1306-1313.
14. M. Andreetto et al., "Combining haptic and bang-bang braking actions for passive robotic walker path following," *IEEE Transactions on Haptics*, Vol. 12, 2019, pp. 542-553.
15. A. Bochkovskiy, C. Y. Wang, and H. Liao, "Yolov4: optimal speed and accuracy of

object detection," arXiv preprint arXiv:2004.10934, 2020.
16. M. E. Yabroudi, K. Awedat, R. C. Chabaan, O. Abudayyeh, and I. Abdel-Qader, "Adaptive DBSCAN lidar point cloud clustering for autonomous driving applications," *IEEE International Conference on Electro Information Technology*, 2022, pp. 221-224.
17. S. Chopra, G. Notarstefano, M. Rice, and M. Egerstedt, "A distributed version of the Hungarian method for multirobot assignment," *IEEE Transactions on Robotics*, Vol. 33, 2017, pp. 932-947.
18. X. Weng, J. Wang, D. Held, and K. Kitani, "3D multi-object tracking: a baseline and new evaluation metrics," *IEEE/RSJ International Conference on Intelligent Robots and Systems*, 2020, pp. 10359-10366.
19. D. Chugo et al., "A dynamic personal space of a pedestrian for a personal mobility vehicle," *IEEE International Conference on Cognitive Infocommunications*, 2013, pp. 223-228.
20. M. R. Batista, D. G. Macharet, and R. A. F. Romero, "Socially acceptable navigation of people with multi-robot teams," *Journal of Intelligent and Robotic Systems*, Vol. 98, 2020, pp. 481-510.
21. M. Missura and M. Bennewitz, "Predictive collision avoidance for the dynamic window approach," *International Conference on Robotics and Automation*, 2019, pp. 8620-8626.
22. H. Yang, X. Xu, and J. Hong, "Automatic parking path planning of tracked vehicle based on improved A* and DWA algorithms," *IEEE Transactions on Transportation Electrification*, Vol. 9, 2022, pp. 283-292.
23. "Pedsim_ros," 2022. Available: https://github.com/srl-freiburg/pedsim_ros.
24. B. Anvari and H. A. Wurdemann, "Modelling social interaction between humans and service robots in large public spaces," *IEEE/RSJ International Conference on Intelligent Robots and* Systems, 2020, pp. 11189-11196.
25. J. V. D. Berg, S. J. Guy, M. Lin, and D. Manocha, "Reciprocal n-body collision avoidance," *Robotics Research*, Vol. 70, 2011, pp. 3-19.
26. J. Brooke, "SUS - A quick and dirty usability scale," *Usability Evaluation in Industry*, Vol. 189, 1996, pp. 189-194.

Shih-Hsing Liu (**劉士興**) received his B.S. degree in electronic and computer engineering from the National Taiwan University of Science and Technology, Taipei, Taiwan, in 2018, and subsequently received his M.S. degree in electrical control engineering from National Yang Ming Chiao Tung University, Hsinchu, Taiwan, in 2021. His research interests include mobile robots, human machine interaction, and embedded systems.

Chien-Yu Su (蘇建宇) received the B.S. degree in electrical engineering from National Taipei University, New Taipei City, Taiwan, in 2018. He is currently pursuing the Ph.D. degree in electrical and computer engineering at National Yang Ming Chiao Tung University, Hsinchu, Taiwan. In 2018, he received the excellent paper award at IEEE International Conference on System Science and Engineering. His research interests include mobile robot manipulator, human machine interaction, assistive robot, and machine learning.

Chun-Hsu Ko (柯春旭) received the M.S. degree in power mechanical engineering from National Tsing Hua University, Hsinchu, Taiwan, in 1991, and the Ph.D. degree in electrical control engineering from National Yang Ming Chiao Tung University, Hsinchu, Taiwan, in 2003. From 1994 to 1998, he was with the Industrial Technology Research Institute, Hsinchu, Taiwan, as an Associate Researcher. He is currently a Professor in the department of Electrical Engineering, I-Shou University, Kaohsiung, Taiwan. His research interests include robot control, robot walking helper, and optimization.

Kuu-young Young (楊谷洋) (M'86–SM'04) was born in Kaohsiung, Taiwan, 1961. He received his B.S. degree in electrical engineering from National Taiwan University, Taiwan, in 1983, and M.S. and Ph.D. degrees in electrical engineering from Northwestern University, Evanston, IL, U.S.A., in 1987 and 1990, respectively. Since 1990, he has been with the department of Electrical Engineering at National Yang Ming Chiao Tung University, Hsinchu, Taiwan, where he is currently a Professor. He served as the chairman of the department from 2003 to 2006, and the associate dean of Electrical and Computer Engineering College, NYCU, from 2007 to 2010 and also 2014 to 2015. His research interests include robot compliance control, robot learning control, robot calibration and path planning, teleoperation, and assistive robot.